First-principles study of the structural, electronic, and optical properties of Ga_2O_3 in its monoclinic and hexagonal phases

Haiying He, Roberto Orlando,* Miguel A. Blanco,† and Ravindra Pandey‡
Department of Physics, Michigan Technological University, Houghton, Michigan 49931, USA

Emilie Amzallag, Isabelle Baraille, and Michel Rérat
Laboratoire de Chimie Théorique et Physico-Chimie Moléculaire, UMR5624 FR-IPREM2606 (CNRS), Université de Pau et des Pays de l'Adour, France

(Received 28 August 2006; published 27 November 2006)

We report the results of a comprehensive study on the structural, electronic, and optical properties of Ga_2O_3 in its ambient, monoclinic (β) and high-pressure, hexagonal (α) phases in the framework of all-electron density functional theory. In both phases, the conduction band minimum is at the zone center while the valance band maximum is rather flat in the k space. The calculated electron effective mass m_e^*/m_0 comes out to be 0.342 and 0.276 for β-Ga_2O_3 and α-Ga_2O_3, respectively. The dynamic dielectric function, reflectance, and energy-loss function for both phases are reported for a wide energy range of 0–50 eV. The subtle differences in electronic and optical properties can be attributed to the higher symmetry, coordination number of Ga atoms, and packing density in α-Ga_2O_3 relative to that in β-Ga_2O_3.

DOI: 10.1103/PhysRevB.74.195123 PACS number(s): 71.20.Nr, 78.20.Ci

I. INTRODUCTION

Gallium oxide (Ga_2O_3) is an important wide-band-gap semiconductor having a wide range of applications from semiconducting lasers,[1] field-effect devices,[2] and switching memories[3] to high-temperature gas sensors.[4,5] The interest in its electronic and optical properties has recently increased because of its potential application as an ultraviolet transparent conducting oxide (TCO).[6–11] TCOs are widely used as transparent electrodes for flat panel displays and solar cells, and phase shift masks for laser lithography. Ga_2O_3 has also drawn attention for its potential application as an antireflection coating.[11,12] The value of its refractive index (1.8–1.9) is close to the square root of that of most III-V semiconductors, which makes it an ideal single-layer antireflection coating for III-V semiconductors. For example, reflectivities as low as 10^{-5} for Ga_2O_3/GaAs structures have been reported.[12] In view of the technological applications of Ga_2O_3 low-dimensional nanostructures,[13] the studies on Ga_2O_3 atomic clusters has also been revived.[14,15]

Ga_2O_3 occurs in the monoclinic (i.e., β) phase at ambient conditions, although it can be transformed into four other high-pressure and temperature polymorphs.[16–18] It is observed to undergo a transition to the hexagonal α-Ga_2O_3 phase at 4.4 GPa, 1000 °C.[19] After quenching to room temperature and pressure, α-Ga_2O_3 remains in a metastable phase. The nanostructures of Ga_2O_3 are also found to be in the α phase.[20] Only β-Ga_2O_3 is extensively studied experimentally[21–27] and less extensively studied theoretically for the electronic structure of its bulk[28–32] and surfaces,[33] the optical absorption,[31] and the energetics and migration of point defects in β-Ga_2O_3.[34] On the other hand, despite it being one of the important phases of Ga_2O_3, experimental studies on α-Ga_2O_3 are rather scarce. To the best of our knowledge, α-Ga_2O_3 has not been studied theoretically. In this paper, we have performed a comprehensive study of α- and β-Ga_2O_3 calculating their structural, electronic, and optical properties using all-electron density functional theory.

The rest of this paper is organized as follows. In Sec. II, we describe the computational details for electronic structure calculations and theoretical framework for calculations of the dielectric constant and other optical properties. The calculated results are presented and discussed in Sec. III. Finally we provide a brief summary in Sec. IV.

II. COMPUTATIONAL METHOD

All-electron density functional theory (DFT) calculations were performed in the framework of the periodic linear combination of atomic orbitals (LCAO) approximation. In the LCAO-DFT approximation, a linear combination of Gaussian orbitals is used to construct a localized atomic basis from which Bloch functions are constructed by a further linear combination with phase factors. All-electron basis sets[35] were adopted in the present study with six s-, five p-, and two d-type shells for Ga (i.e., a 864111/64111/41 set) and four s, three p, and one d-type shells for O (i.e., a 8411/411/1 set). The exponent (in units of bohr^{-2}) of the most diffuse sp shell was reoptimized to be 0.225 and 0.200 for Ga and O, respectively. The exchange and correlation effects were treated by the B3LYP functional form (i.e., Becke's three-parameter hybrid exchange functional[36] and Lee, Yang, and Parr correlation functional[37] as implemented in the program package CRYSTAL03.[38] We note here that DFT calculations employing the B3LYP functional form have been reported to yield band gaps which are in good agreement with the corresponding experimental values.[39,40] The Brillouin zone is sampled using a $4\times4\times4$ Monkhorst net for integration in the reciprocal space. We set the total energy tolerance to 10^{-7} hartree and eigenvalue tolerance to 10^{-6} hartree in the iterative solution of the Kohn-Sham equations. The level of accuracy in evaluating the Coulomb and Hartree-Fock exchange series is controlled by five

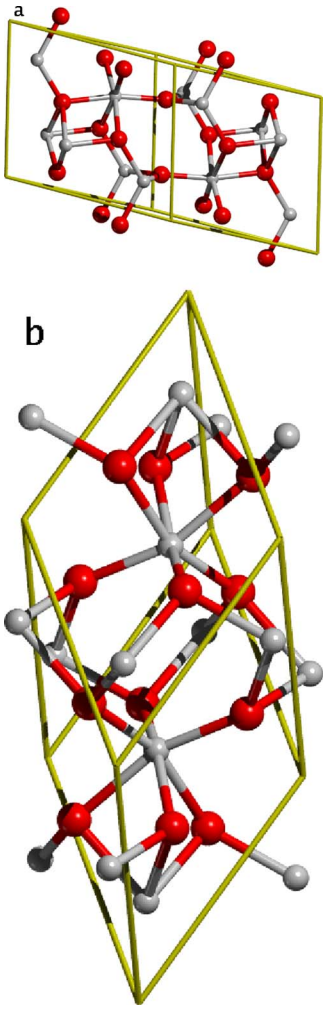

FIG. 1. (Color online) Illustration of crystalline structures of (a) β-Ga_2O_3 and (b) α-Ga_2O_3. Ga atoms are in gray (gray) and O atoms in red (black). The primitive cells are also shown.

parameters,[38] for which standard values given in CRYSTAL (i.e., 6 6 6 6 12) have been used.

The sum over states (SOS) method is used to calculate the real and imaginary parts of the mean dynamic polarizabilty $[\alpha(\omega)]$ as a function of the electric field frequency (ω).[41] The polarizability can be expressed as follows:

$$\alpha(\omega) = \sum_k \Omega_k \sum_{i,j} f_{ij\vec{k}} \left[\frac{\Delta\epsilon_{ij\vec{k}}^2 - \omega^2 + i\eta\omega}{(\Delta\epsilon_{ij\vec{k}}^2 - \omega^2)^2 + \omega^2\eta^2} \right]. \quad (1)$$

$f_{ij\vec{k}}$ are oscillator strengths between valence $|i\rangle$ (occupied) and conduction $|j\rangle$ (unoccupied) crystalline orbitals for each $\vec{k}$ point with a geometric weight Ω_k; $\Delta\epsilon_{ij\vec{k}}$ are the corresponding vertical transition energies $\epsilon_{j\vec{k}} - \epsilon_{i\vec{k}}$; and η is the damping factor which corresponds to an average value of the inverse of lifetime of the excited states. A common value of η=0.3 eV corresponding approximately to the experimental resolution was used. Without η, there would be many resonances in the spectrum of dielectric constant.

Assuming that the wavelength of the electric field is much larger than the Bohr length (a_0), the oscillator strength in the dipole approximation can be expressed as

$$f_{ij\vec{k}} = (2/3)(\epsilon_{j\vec{k}} - \epsilon_{i\vec{k}})\langle i|\vec{r}|j\rangle_{\vec{k}}^2. \quad (2)$$

In this work, as in a previous study on nitrides,[42] the velocity operator was used, and the transition moments $\langle i|\vec{r}|j\rangle_{\vec{k}}$ were replaced by $\langle i|\vec{\nabla}|j\rangle_{\vec{k}}/(\epsilon_{j\vec{k}} - \epsilon_{i\vec{k}})$, as if the hypervirial theorem was checked. No scissor operator was used to correct the transition energies, but the oscillator strengths for each $\vec{k}$ point were multiplied by a factor such that their sum over valence occupied orbitals is equal to the number of valence electrons in the cell to obey the so-called Thomas-Reiche-Kuhn rule.

The dielectric constant ϵ can be approximated as

$$\epsilon(\omega) = 1 + 4\pi N\alpha(\omega), \quad (3)$$

where N is the number of moieties per unit volume. From this, the dynamic reflectance takes the expression

$$R(\omega) = \frac{[1 - \mathrm{Re}(\sqrt{\epsilon(\omega)})]^2 + [\mathrm{Im}(\sqrt{\epsilon(\omega)})]^2}{[1 + \mathrm{Re}(\sqrt{\epsilon(\omega)})]^2 + [\mathrm{Im}(\sqrt{\epsilon(\omega)})]^2}, \quad (4)$$

while the energy-loss function (ELF) is

$$\mathrm{ELF}(\omega) = \mathrm{Im}\left(-\frac{1}{\epsilon(\omega)}\right). \quad (5)$$

III. RESULTS AND DISCUSSION

A. Structural properties

The monoclinic phase of Ga_2O_3 [Fig. 1(a)] has $C2/m$ symmetry with four formula units per crystallographic cell, and is characterized by four lattice parameters, namely a, b, c, and β.[43] In the lattice unit cell, there are two crystallographically nonequivalent Ga atoms, and three nonequivalent O atoms, all of them located at $4i(x,0,z)$ positions, at a symmetry plane (C_s group). Therefore, there are 14 degrees of freedom to be considered during geometry optimization calculations. The Ga atoms have tetrahedral- and octahedral-like coordinations in the lattice. The crystalline structure can be described in terms of GaO_6 octahedra and GaO_4 tetrahedra: there are zigzag double chains of edge-sharing GaO_6 octahedra, linked by single chains of vertex-sharing GaO_4 tetrahedra along the **b** axis.

α-Ga_2O_3 [Fig. 1(b)] has the corundum structure with $R\bar{3}c$ symmetry. The crystallographic cell consists of six Ga_2O_3 formula units. It has two independent lattice parameters a and c, and two internal coordinate variables z_{Ga} and x_O. The oxygen ions are approximately hexagonal close packed and the gallium ions occupy two-thirds of the octahedral sites. Each Ga octahedron shares one face and three edges with three other octahedra; the Ga octahedra are moderately distorted in the lattice.

Figure 2 shows the calculated potential energy curves (i.e., total energy vs volume) of α- and β-Ga_2O_3, where the lattice parameters as well as the internal coordinates are optimized at each fixed value of crystallographic unit-cell volume for both phases. The calculated energy surface is used to compute the $V(P)$ equation of state, which is then fitted to Vinet analytic form[44] yielding the equilibrium cell volume,

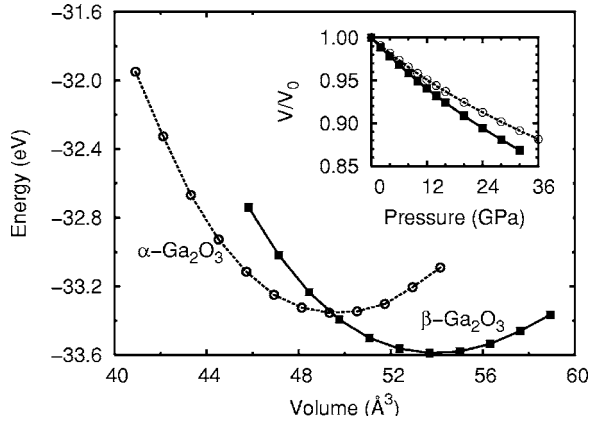

FIG. 2. Energy vs volume per formula unit of β-Ga_2O_3 and α-Ga_2O_3. V/V_0 vs pressure is given in the inset, together with the fitted equation of state.

bulk modulus (B_0), and its pressure derivative (B_0').

The structural parameters corresponding to the equilibrium geometry are listed in Table I. Overall, the agreement between the calculated and the corresponding experimental values is very good. The calculated equilibrium cell volume in both phases is about 3% larger as compared to the corresponding experimental value. The calculated bulk modulus of the high-pressure, α-Ga_2O_3 phase (B_0=210 GPa, B_0'=4.95) is significantly higher than that of the ambient phase, β-Ga_2O_3 (B_0=174 GPa, B_0'=3.79), as we would expect. The calculated binding energy of Ga_2O_3 with respect to the constituent atoms is 33.6 and 33.3 eV per formula unit for β-Ga_2O_3 and α-Ga_2O_3, respectively. The energy difference of 0.3 eV between β-Ga_2O_3 and α-Ga_2O_3 is in the range of 1.15–0.17 eV predicted by Albanesi *et al.*[28] for the difference in tetrahedral and octahedral sites using a semiempirical model. Using a static estimate from the $E(V)$ curvature,[45] the Debye temperature Θ_D of β-Ga_2O_3 and α-Ga_2O_3 is predicted to be 634 and 690 K, respectively. No experimental data are available for comparison with the predicted values.

TABLE I. Lattice constants and internal structural parameters of zero-pressure β-Ga_2O_3 and α-Ga_2O_3.

β-Ga_2O_3			α-Ga_2O_3		
Property	This work	Exp.[a]	Property	This work	Exp.[b]
Lattice parameters			Lattice parameters		
a(Å)	12.34	12.23	a(Å)	5.04	4.983
b(Å)	3.08	3.04	c(Å)	13.56	13.433
c(Å)	5.87	5.80			
β(°)	103.9	103.7			
Fractional coordinates			Fractional coordinates		
x_{Ga_I}	0.091	0.090	z_{Ga}	0.356	0.3554
z_{Ga_I}	0.794	0.795	x_O	0.302	0.3049
$x_{Ga_{II}}$	0.342	0.341			
$z_{Ga_{II}}$	0.686	0.686			
x_{O_I}	0.163	0.167			
z_{O_I}	0.109	0.101			
$x_{O_{II}}$	0.495	0.496			
$z_{O_{II}}$	0.257	0.255			
$x_{O_{III}}$	0.826	0.828			
$z_{O_{III}}$	0.436	0.436			

[a]Experimental results for β-Ga_2O_3 are taken from Ref. 16.
[b]Experimental results for α-Ga_2O_3 are taken from Ref. 17.

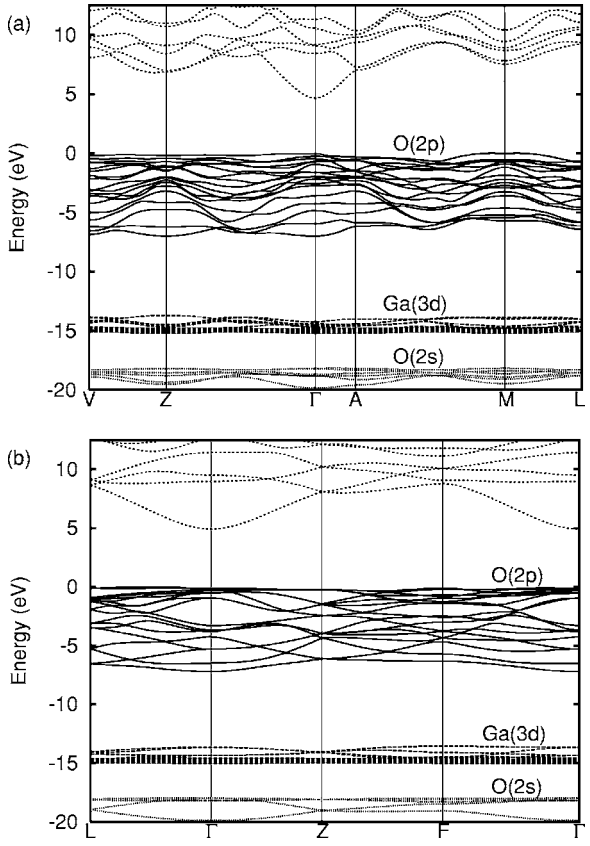

FIG. 3. Band structure of (a) β-Ga_2O_3. The **k** points are $\Gamma=(000)$, $A=(00\frac{1}{2})$, $Z=(\frac{1}{2}\frac{1}{2}0)$, $M=(\frac{1}{2}\frac{1}{2}\frac{1}{2})$, $L=(0\frac{1}{2}\frac{1}{2})$, and $V=(0\frac{1}{2}0)$; (b) α-Ga_2O_3, the **k** points are $\Gamma=(000)$, $L=(0\frac{1}{2}0)$, $Z=(\frac{1}{2}\frac{1}{2}\frac{1}{2})$, $F=(\frac{1}{2}\frac{1}{2}0)$. The top of the valence band is aligned to zero.

At zero pressure, the equilibrium unit cell volume of the α phase relative to that of the β phase turns out to be 0.92. From the calculated density of β-Ga_2O_3 and α-Ga_2O_3 (5.757 and 6.273 g/cm^3), it is expected that the α phase would be stable at high pressure, as experiments have found out. Consistently, as we have stated above, higher B_0, B_0', and Θ_D are also found for the high-pressure α phase. From the $\Delta G_{static}(P_{tr})=0$ condition for the energy surfaces shown in Fig. 2, we determine the phase transition pressure to be 9.5 GPa, associated with a volume for the α phase of 47.620 Å^3 and for the β phase of 51.285 Å^3 per formula unit. It is comparable with the transition pressure of 4.4 GPa measured at a high temperature (1000 °C).[19]

B. Electronic structure

Figure 3 displays the upper valence and lower conduction band structure of β- and α-Ga_2O_3 at zero pressure. We will

focus on zero-pressure structures for β and α phases from now on. The results of β-Ga_2O_3 are in good agreement with previous studies using the pseudopotential-plane wave approach[32] and the full-potential linearized augmented plane wave method.[31] Anionic and cationic states constitute the top of the valence and the bottom of the conduction band, respectively. In general, the band structures of these two phases are very similar. The uppermost valence band is mainly formed by O $2p$ states, with a width of about 7.01 and 7.10 eV for β- and α-Ga_2O_3, respectively. Note that both the band structures are plotted for primitive cells with the same number of atoms per cell, namely 4 Ga atoms and 6 O atoms. As the symmetry increases from monoclinic (β phase) to hexagonal (α phase), more eigenstates become degenerate. We can clearly see this from the plotted band structures in Fig. 3. For example, the 18 O $2p$ subbands are grouped into six eigenvalues at the Z k point for α-Ga_2O_3.

The valence band maximum appears to be almost degenerate at the Γ and M **k** points for β-Ga_2O_3; the energy at Γ being 0.03 eV lower than that at M. On the other hand, the conduction band minimum occurs at Γ, so there is a direct gap of 4.69 eV at Γ and an indirect M-Γ gap of 4.66 eV, in good agreement with optical absorption measurements.[46] Our calculations show another successful case in employing the B3LYP hybrid functional form and local atomic basis sets in reproducing the band gap of wide-band-gap semiconductors, which, however, has been a notorious problem of underestimating band gaps in LDA and GGA calculations. Our theoretical results also shed light on the obscurity in the nature of the band gap.[11,24] In single crystals of β-Ga_2O_3, experimental measurements have reported an absorption edge at 4.60 eV or 2700 Å at room temperature, which shifts to 4.78 eV or 2600 Å when the temperature is reduced to 77 K. A recent experimental study[6] finds the absorption edge to be at 4.79 and 4.52 eV for light polarized along the **b** and **c** axes, respectively. Finally, our calculations do not predict a closing of the energy gap, at least up to 40 GPa, in the monoclinic Ga_2O_3.

In α-Ga_2O_3, the top of the valence band is only about 0.05 eV lower at Γ than at L or F **k** points. It leads to a direct gap of 5.08 eV at Γ and an indirect L-Γ or F-Γ gap of 5.03 eV. A recent study on α-Ga_2O_3 nanocrystalline thin films revealed its optical band gap to be 4.98 eV, as determined from transmittance measurements.[20]

All-electron calculations allow us to calculate bands associated with the core electron levels accurately, which provide important information in identifying the rearrangement of elemental electronic structure levels in a compound by XPS experiments. There are two relatively narrow bands at about 14 (Ga $3d$) and 18 eV (O $2s$) below the valence band maximum in both phases. On the other hand, x-ray photoelectron spectroscopy (XPS) measurements of polycrystalline β-Ga_2O_3 reported a Ga $3d$ binding energy of 20.4 eV, associated with a peak whose half-width is 1.73 eV.[28] Considering the band gap as a rough approximation for the energy required to eject an electron from the top of the valence band, the location of the top of Ga-$3d$ band relative to the top of the valence band comes out to be 15.7 eV, which is in reasonable agreement with the calculated value of 14.2 eV. The half-width of the XPS peak is also in good agreement of our calculated value of 1.53 eV.

The valence band is almost flat in both phases of Ga_2O_3, indicating a rather large effective mass for holes. On the other hand, the calculated average values of electron effective mass m_e^*/m_0 are 0.342 and 0.276 for β-Ga_2O_3 and α-Ga_2O_3, respectively. The effective mass values were obtained by fitting the energy dispersion of the conduction band minimum to a parabolic function along different **k** directions in the vicinity of Γ. The values of effective electron mass are practically isotropic, which agrees with a recent theoretical study by Yamaguchi.[31] It was pointed out that the observed anisotropy in the n-type semiconducting state should not be attributed to the properties of a perfect lattice.[31] Although electron effective mass is a key transport property for semiconductors, it has not been measured accurately in Ga_2O_3. It is only estimated to be 0.5–2.0 m_0 for β-Ga_2O_3.[6] Similarly, the average electron effective mass of α-Al_2O_3 is estimated to be 0.35 m_0.[47] The calculated effective mass values of Ga_2O_3 are comparable to those associated with most semiconducting materials, suggesting that the electronic conduction in Ga_2O_3 is possible only if the electrons can be promoted to the conduction band by overcoming the relatively larger band gap.

Electronic structure calculations can also predict the nature and location of interband transitions in a crystal, which will assist the experimentalists in identifying the peaks in the optical spectra obtained by either reflectance or x-ray photoelectron spectroscopy. In β-Ga_2O_3, a group of peaks at 2.37, 2.65, and 2.83 eV relative to the gap at Γ are predicted, which are associated with interband transitions from the top of the valence band to the bottom of the conduction band at Z, A, and M **k** points, respectively. This group is followed by two peaks at 3.59 and 5.23 eV, associated with V and L **k** points. Similarly, there are three peaks at 3.25, 3.68, and 3.83 eV associated with Z, L, and F **k** points, respectively, relative to the gap at Γ in α-Ga_2O_3.

C. Optical properties

The dielectric function, $\epsilon(\omega)$ can be used to describe the linear response of the system to an electromagnetic radiation, which is related to the interaction of photons with electrons. Of the two contributions to $\epsilon(\omega)$, namely intraband and interband transitions, contributions from the intraband transitions are ignored in calculations as they are shown to be important only for metals. The calculated gap of Ga_2O_3 is about 4.7 eV. A sum over states (SOS) method is used to calculate the real and imaginary parts of the polarizability, α. The real and imaginary parts of dielectric function $\epsilon_1(\omega)$ and $\epsilon_2(\omega)$ can then be analytically and separately deduced without performing numerical integration according to the Kramers-Kronig transformation.[50]

The calculated values of the optical dielectric constant, ϵ, are listed in Table II together with the refractive index $n=\sqrt{\epsilon}$ for both β- and α-Ga_2O_3 at zero pressure. Note that ϵ is obtained from the zero-frequency limit of $\epsilon_1(\omega)$, and it corresponds to the electronic part of the static dielectric constant of the material, a parameter of fundamental importance in many aspects of materials properties. Since the calculated dielectric tensor is almost isotropic, the mean value of ϵ,

TABLE II. Optical dielectric constant, refractive index, and reflectivity of β-Ga_2O_3 and α-Ga_2O_3.

	β-Ga_2O_3		α-Ga_2O_3	
	This work	Exp.	This work	Exp.
ϵ_{xx}	2.78		3.07	
ϵ_{yy}	2.84		3.07	
ϵ_{zz}	2.86		2.97	
$\bar{\epsilon}$	2.82	3.57[a], 3.38, 3.53[b]	3.03	3.69, 3.80[c]
$\bar{n}$	1.68	1.89[a], 1.84, 1.88[b]	1.74	1.92, 1.95[c]

[a]From Ref. 48.
[b]From Ref. 12.
[c]From Ref. 49.

together with that of n is also given in Table II. It is to be noted here that calculations of ϵ and n are also performed with a relatively more accurate "coupled" method,[38] which introduces a finite field (FF) perturbation in the self-consistent field (SCF) cycle as a "sawtooth" electric potential to keep the periodicity of the system. This coupled FF method takes into account the so-called local field effects.[51,52] The agreement between the FF and SCF values is good. For example, the static value of the refractive index n obtained by the SOS method is 1.74 whereas that obtained by the FF method is 1.82 for α-Ga_2O_3.

When we compare our results with experimental ones, we should keep in mind that our calculations are essentially for a perfect static crystal (zero temperature and neglecting zero point vibrations), while the experimental measurement may be affected by the presence of phonons at finite temperature and the contamination with defects or impurities. The calculated values of n are about 10% smaller than the experimental values in both α- and β-Ga_2O_3. We should also be aware of the fact that only pseudo-eigenvalues are available in the DFT approximation. It might be an error source for the application of equations involving energy eigenvalues, like Eqs. (1) and (2), for example. Note also that the experimental values of β-Ga_2O_3 are for thin films. On the other hand, the calculated gap energy being in good agreement with the experimental one, the prediction for the dispersion of the dielectric constant should be accurate and reliable till the first resonance in the spectrum.

The dielectric constant is directly related to the polarizability of the crystal. The polarizability, which represents the deformability of the electronic distribution, is to be connected with the shape of the valence charge density. In such a highly ionic material as Ga_2O_3, oxygen ions are expected to provide the largest contribution to polarizability. They are located in a distorted hexagonal close-packed array in α-Ga_2O_3, while loosely following a cubic close-packed array in β-Ga_2O_3. A similarity in dielectric as well as optical properties between β- and α-Ga_2O_3 is expected, as was predicted in the present study. A slightly larger dielectric constant of α-Ga_2O_3 relative to β-Ga_2O_3 may be traced to the slightly denser packing of ions and higher coordination number of Ga atoms in the α-Ga_2O_3 lattice.

The $\epsilon_1(\omega)$ and $\epsilon_2(\omega)$ components for both β-Ga_2O_3 and α-Ga_2O_3 are plotted in Figs. 4 and 5 in a wide range of energy, 0–50 eV. Their similarity is a direct reflection of the similarity in the band structures shown in Fig. 3. It is an advantageous attempt of theoretical studies to identify the transitions that are responsible for the peaks in $\epsilon_2(\omega)$ using the calculated band structures. The major band located around 12 eV is attributed to the interband transitions from O-2p valence band to Ga-4s conduction band. This band has more pronounced peaks in α-Ga_2O_3 due to its higher degeneracy. The smaller peak at 20 eV is originated by the excitation of Ga-3d electrons to the Ga-4s conduction orbitals.

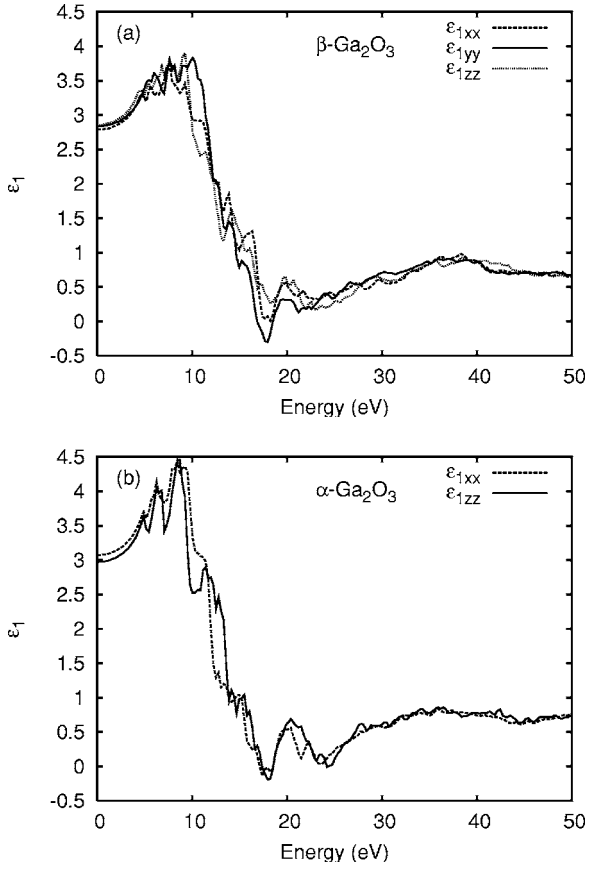

FIG. 4. Real part of dielectric function for (a) β-Ga_2O_3 and (b) α-Ga_2O_3.

Concerning anisotropy, the dispersion ϵ_{xx} (ϵ_{yy}) function of the more symmetric α-Ga_2O_3 phase, which has hexagonal symmetry, can be distinguished from ϵ_{zz}, the allowed transitions being different (see the comparative real and imaginary parts plotted in Figs. 4 and 5). Nevertheless, anisotropy in the dynamic dielectric function, especially in the range of 10–20 eV, is also observed for β-Ga_2O_3. The ϵ_{yy} component is distinguishable from ϵ_{xx} and ϵ_{zz}, as being closely related to the chain-type structure along the b axis.[16] In particular, the optical absorption edge, identified as an abrupt slope in ϵ_2 in Fig. 5, does show a significant anisotropy along the x/z and y axis, with an energy difference of 0.6 eV. It is in good agreement with the experimental value of 0.3 eV,[6] and a previous theoretical result of 0.7 eV.[31] α-Ga_2O_3, however, does not show any obvious difference in the absorption edge along different directions.

The variation of reflectance as a function of photon frequency is displayed in Fig. 6. The dynamic reflectance cor-

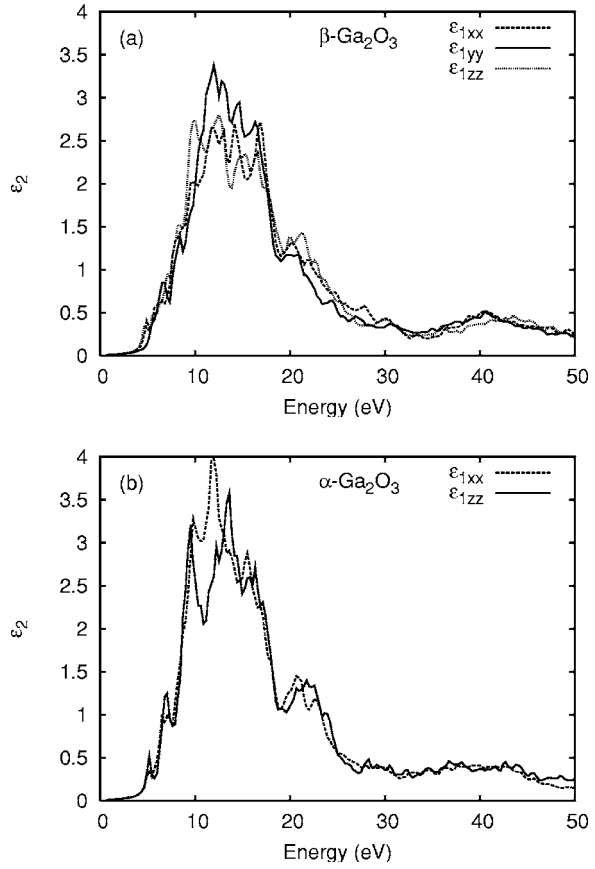

FIG. 5. Imaginary part of dielectric function for (a) β-Ga_2O_3 and (b) α-Ga_2O_3.

responds to the ratio of the intensities of the incident and reflected electric fields. In the low energy regime ($\leqslant$6 eV), the reflectance curves are nearly flat with reflectivity values of 0.06 and 0.07 for β-Ga_2O_3 and α-Ga_2O_3, respectively. The small value of reflectance ensures its applications as transparent coatings in the visible to deep UV light regime. α-Ga_2O_3 shows an overall larger reflectance and a broader band in the range of 10–30 eV than β-Ga_2O_3. The reflectance in the energy range of 0–50 eV presented in this study could serve as a reference for future experimental studies on Ga_2O_3.

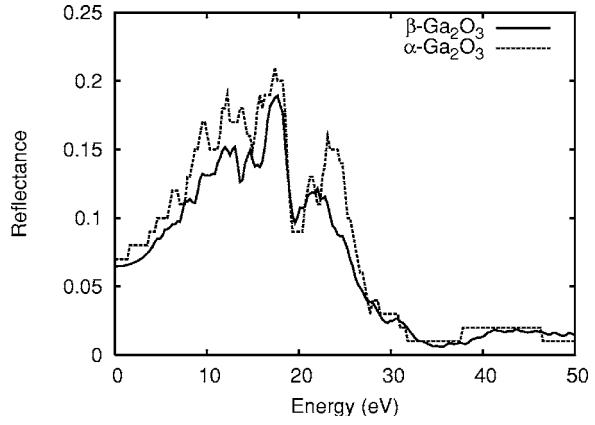

FIG. 6. Simulated reflectance spectra of β-Ga_2O_3 and α-Ga_2O_3.

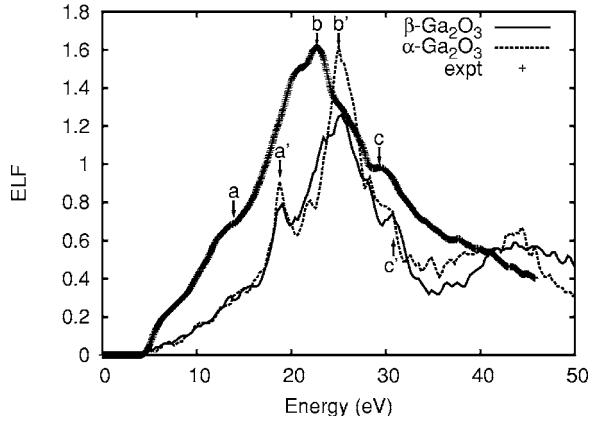

FIG. 7. Energy-loss function for β-Ga_2O_3 and α-Ga_2O_3. The experimental data taken from Schamm *et al.* (Ref. 53) are plotted as plus signs and scaled to match the calculated peak maximum.

At small scattering angles, the energy-loss function (ELF) is deduced from the dynamic dielectric constant using Eq. (5). The ELF spectra clearly show the energy ranges corresponding to the electronic excitations of the different orbitals. This function is important because it allows us to compare the theoretical results with spectroscopy (e.g., EELS, EXELF) measurements which provide information about the electronic system interacting with an incident electron beam. As shown in Fig. 7, the shape of the calculated ELF spectra is very similar to that of the experimental result.[53] A broad band appears in the energy range from 5 to 35 eV. However, the peak positions in the energy scale are shifted towards higher energies relative to those in the experimental spectrum. The three pronounced peaks (a, b, and c in Fig. 7) located at 13.9, 22.7, and 29.3 eV in the experimental spectrum are shifted to 19.0/18.8, 25.3/25.0, and 30.8/30.8 eV (peaks a', b', and c' in Fig. 7) in β/α phases. It is to be noted that the experimental data were obtained for thin layers and temperature effects (vibration) may also become important in the experimental conditions.

A significant feature in the low-loss spectrum ($<$50 eV) is the bulk plasmon peak, which has an intensity several orders of magnitude higher than the core-loss edges due to collective oscillation of the loosely bound electrons, which runs as a longitudinal wave through the volume of the crystal with a characteristic frequency. The plasmon energy obtained from the highest peak position is 25.3 and 25.0 eV for β-Ga_2O_3 and α-Ga_2O_3, respectively. The corresponding experimental value is 22.7 eV.[53]

IV. SUMMARY

The potential use of Ga_2O_3 in the form of low-dimensional nanostructures has triggered interest in studying its metastable phase (α) as well as its ambient phase (β). In the present study, an all-electron density functional theory approach has been used to investigate the structural, electronic, and optical properties of both the β (monoclinic) and α (hexagonal) phases. The dynamic dielectric function, reflectance, and energy-loss function for both phases were re-

ported for a wide energy range of 0–50 eV. A good agreement has been achieved for β-Ga_2O_3 whenever experimental results or previous theoretical studies are available. We believe that the properties of α-Ga_2O_3 can also be predicted accurately on the same footing, which may supply important guidance in the technological applications.

Our calculations show a high pressure phase transition at about 9.5 GPa from β-Ga_2O_3 to α-Ga_2O_3. Although the overall properties of α-Ga_2O_3 remain more or less the same as those of β-Ga_2O_3, differences arise due to the higher symmetry, coordination number of Ga atoms, and packing density in α-Ga_2O_3. The high-pressure phase α-Ga_2O_3 has shown a higher bulk modulus, Debye temperature, band gap, refractive index, and reflectance. Its high symmetry has led to more degeneracy in its electronic band structure. An indirect band gap of 5.03 eV and a relatively low effective mass of 0.276 m_0 were obtained. The anisotropy in the dispersion ϵ_{xx} (ϵ_{yy}) function with respect to ϵ_{zz} is more pronounced than in the case of β-Ga_2O_3. It does not, however, show anisotropy in the optical absorption edge as in β-Ga_2O_3.

ACKNOWLEDGMENTS

We thank S. Gowtham for help with computational facilities and Piero Uglieongo for help with graphics. Funding from Spanish DGICyT Grant No. BQU2003-06553 is acknowledged. Sylvie Schamm is acknowledged for fruitful discussions, and the experimental EELS data she sent to us that are reported in Fig. 7.

*Permanent address: Dipartimento di Scienze e Tecnologie Avanzate, Università del Piemonte Orientale, Via Bellini 25/G, 15100 Alessandria, Italy.

†Permanent address: Departamento de Química Física y Analítica, Universidad de Oviedo. Oviedo 33006, Spain.

‡Corresponding author. Electronic address: pandey@mtu.edu

[1] M. Passlacki, M. Hong, and J. P. Mannaerts, Appl. Phys. Lett. **68**, 1099 (1996).

[2] Z. Li, C. de Groot, J. Jagadeesh, and H. Moodera, Appl. Phys. Lett. **77**, 3630 (2000).

[3] L. Binet and D. Gourier, J. Phys. Chem. Solids **59**, 1241 (1998).

[4] M. Fleischer and H. Meixner, J. Appl. Phys. **74**, 300 (1993).

[5] K. Bernhardt, M. Fleischer, and H. Meixner, Siemens Forsch.-Entwicklungsber. **30**, 35 (1995).

[6] N. Ueda, H. Hosono, R. Waseda, and H. Kawazoe, Appl. Phys. Lett. **70**, 3561 (1997).

[7] D. D. Edwards, P. E. Folkins, and T. O. Mason, J. Am. Ceram. Soc. **80**, 253 (1997).

[8] N. Ueda, H. Hosono, R. Waseda, and H. Kawazoe, Appl. Phys. Lett. **71**, 933 (1997).

[9] D. D. Edwards, T. O. Mason, F. Goutenoire, and K. R. Poeppelmeier, Appl. Phys. Lett. **70**, 1706 (1997).

[10] M. Orita, H. Hiramatsu, H. Ohta, M. Hirano, and H. Hosono, Thin Solid Films **411**, 134 (2002).

[11] F. K. Shan, G. X. Liu, W. J. Lee, G. H. Lee, I. S. Kim, and B. C. Shin, J. Appl. Phys. **98**, 023504 (2005).

[12] M. Passlacki, E. F. Schubert, W. S. Hobson, M. Hong, N. Moriya, S. Chu, K. Konstadinidis, J. P. Mannaerts, M. L. Schnoes, and G. J. Zydzik, J. Appl. Phys. **77**, 686 (1995).

[13] Z. L. Wang, Annu. Rev. Phys. Chem. **55**, 159 (2004).

[14] S. Gowtham, A. Costales, and R. Pandey, J. Phys. Chem. B **108**, 17295 (2004).

[15] S. Gowtham, M. Deshpande, A. Costales, and R. Pandey, J. Phys. Chem. B **109**, 14836 (2005).

[16] S. Geller, J. Chem. Phys. **33**, 676 (1960).

[17] M. Marezio and J. P. Remeika, J. Chem. Phys. **46**, 1862 (1967).

[18] D. F. Edwards, *Handbook of Optical Constants of Solids* (Academic Press, New York, 1998), Vol. III, p. 753.

[19] J. P. Remeika and M. Marezio, J. Am. Chem. Soc. **8**, 87 (1966).

[20] G. Sinha, K. Adhikary, and S. Chaudhuri, J. Cryst. Growth **276**, 204 (2005).

[21] X. Wu, W. Song, W. Huang, M. Pu, B. Zhao, Y. Sun, and J. Du, Chem. Phys. Lett. **328**, 5 (2000).

[22] G. Park, W. Choi, J. Kim, Y. Choi, Y. Lee, and C. Lim, J. Cryst. Growth **220**, 494 (2000).

[23] W. Han, P. Kohler-Redlich, F. Ernst, and M. Rühle, Solid State Commun. **115**, 527 (2000).

[24] M. Orita, H. Ohta, and M. Hirano, Appl. Phys. Lett. **77**, 4166 (2000).

[25] Z. W. Pan, Z. R. Dai, and Z. L. Wang, Science **291**, 1947 (2001).

[26] C. Liang, G. Meng, G. Wang, Y. Wang, L. Zhang, and S. Zhang, Appl. Phys. Lett. **78**, 3202 (2001).

[27] J. Li, X. Chen, Z. Qiao, M. He, and H. Li, J. Phys.: Condens. Matter **13**, L937 (2001).

[28] E. A. Albanesi, S. J. Sferco, I. Lefebvre, G. Allan, and G. Hollinger, Phys. Rev. B **46**, 13260 (1992).

[29] L. Binet, D. Gourier, and C. Minot, J. Solid State Chem. **113**, 420 (1994).

[30] Z. Hajnal, J. Miró, G. Kiss, F. Réti, P. Deák, R. C. Herndon, and J. M. Kuperberg, J. Appl. Phys. **86**, 3792 (1999).

[31] K. Yamaguchi, Solid State Commun. **131**, 739 (2004).

[32] H. He, M. A. Blanco, and R. Pandey, Appl. Phys. Lett. **88**, 261904 (2006).

[33] V. M. Bermudez, Chem. Phys. **323**, 193 (2006).

[34] M. A. Blanco, M. B. Sahariah, H. Jiang, A. Costales, and R. Pandey, Phys. Rev. B **72**, 184103 (2005).

[35] www.crystal.unito.it/Basis_Sets/gallium.html#86-411d4G for Ga and www.crystal.unito.it/Basis_Sets/oxygen.html#8-411G for O (accessed November 2005).

[36] A. D. Becke, J. Chem. Phys. **98**, 5648 (1993).

[37] C. Lee, W. Yang, and R. G. Parr, Phys. Rev. B **37**, 785 (1998).

[38] V. R. Saunders, R. Dovesi, C. Roetti, R. Orlando, C. M. Zicovich-Wilson, N. M. Harrison, K. Doll, B. Civalleri, I. J. Bush, P. D'Arco, and M. Llunell, CRYSTAL2003 *User's Manual* (University of Torino, Torino, Italy, 2003).

[39] J. Muscat, A. Wander, and N. M. Harrison, Chem. Phys. Lett. **342**, 397 (2001).

[40] H. Jiang, R. Orlando, M. A. Blanco, and R. Pandey, J. Phys.: Condens. Matter **16**, 3081 (2004).

[41] D. Ayma, J. P. Campillo, M. Rérat, and M. Causà, J. Comput.

Chem. **18**, 1253 (1997).
[42] R. Pandey, M. Rérat, C. Darrigan, and M. Causà, J. Appl. Phys. **88**, 6462 (2000).
[43] J. Áhman, G. Svensson, and J. Albertsson, Acta Crystallogr., Sect. C: Cryst. Struct. Commun. **52**, 1336 (1996).
[44] P. Vinet, J. H. Rose, J. Ferrante, and J. R. Smith, J. Phys.: Condens. Matter **1**, 1941 (1989).
[45] M. A. Blanco, E. Francisco, and V. Luaña, Comput. Phys. Commun. **158**, 57 (2004).
[46] H. H. Tippins, Phys. Rev. **140**, A316 (1965).
[47] Y. Xu and W. Y. Ching, Phys. Rev. B **43**, 4461 (1991).
[48] M. Rebien, W. Henrion, M. Hong, J. P. Mannaerts, and M. Fleischer, Appl. Phys. Lett. **81**, 250 (2002).
[49] *CRC Handbook of Chemistry and Physics*, 70th ed., edited by R. C. Weast (CRC, Boca Raton, 1989), p. B-92.
[50] S. D. Mo and W. Y. Ching, Phys. Rev. B **51**, 13023 (1995).
[51] C. Darrigan, M. Rérat, G. Mallia, and R. Dovesi, J. Comput. Chem. **24**, 1305 (2003).
[52] M. Rérat and R. Dovesi, in *International Conference of Computational Methods in Sciences and Engineering (ICCMSE 2004), Lecture Series on Computer and Computational Sciences*, edited by T. Simos and G. Maroulis (Brill Academic, Leiden, The Netherlands, 2004), Vol. 1, p. 771.
[53] S. Schamm and G. Zanchi, Ultramicroscopy **96**, 559 (2003).